Influence of external forces on actin-dependent T cell protrusions during immune synapse formation

Andrés Ernesto Zucchetti, Noémie Paillon, Olga Markova, Stéphanie Dogniaux, Claire Hivroz, Julien Husson

▶ **To cite this version:**

Andrés Ernesto Zucchetti, Noémie Paillon, Olga Markova, Stéphanie Dogniaux, Claire Hivroz, et al.. Influence of external forces on actin-dependent T cell protrusions during immune synapse formation. Biology of the Cell, 2021, 113 (5), pp.250-263. 10.1111/boc.202000133 . hal-04243745

HAL Id: hal-04243745
https://hal.science/hal-04243745

Submitted on 16 Oct 2023

HAL is a multi-disciplinary open access archive for the deposit and dissemination of scientific research documents, whether they are published or not. The documents may come from teaching and research institutions in France or abroad, or from public or private research centers.

L'archive ouverte pluridisciplinaire **HAL**, est destinée au dépôt et à la diffusion de documents scientifiques de niveau recherche, publiés ou non, émanant des établissements d'enseignement et de recherche français ou étrangers, des laboratoires publics ou privés.

Accepted Article

Influence of external forces on actin-dependent T cell protrusions during immune synapse formation

Andrés Ernesto Zucchetti[1], Noémie Paillon[1], Olga Markova[2], Stéphanie Dogniaux[1], Claire Hivroz[1] and Julien Husson[2*]

[1] Institut Curie, PSL Research University, INSERM U932, Integrative analysis of T cell activation team, 26 rue d'Ulm, 75248, Paris Cedex 05, France.

[2] LadHyX, CNRS, Ecole polytechnique, Institut Polytechnique de Paris, 91120, Palaiseau, France.

* corresponding author.

Running title (max 50 char. incl. spaces)

Influence of forces on T cell protrusions

Abstract

Background Information

We have previously observed that in response to antigenic activation T cells produce actin-rich protrusions that generate forces involved in T cell activation. These forces are influenced by the mechanical properties of antigen presenting cells (APCs). However, how external forces, which can be produced by APCs, influence the dynamic of the actin-protrusion remains unknown. In this study, we quantitatively characterized the effects of external forces in the dynamic of the protrusion grown by activated T cells.

Results

Using a micropipette force probe, we applied controlled compressive or pulling forces on primary T lymphocytes activated by an antibody-covered microbead, and measured the effects of these forces on the protrusion generated by T lymphocytes. We found that the application of compressive forces

This article has been accepted for publication and undergone full peer review but has not been through the copyediting, typesetting, pagination and proofreading process, which may lead to differences between this version and the Version of Record. Please cite this article as doi: 10.1111/boc.202000133.

This article is protected by copyright. All rights reserved.

Accepted Article

slightly decreased the length, the time at which the protrusion stops growing and retracts and the velocity of the protrusion formation, whereas pulling forces strongly increased these parameters. In both cases, the applied forces did not alter the time required for the T cells to start growing the protrusion (delay). Exploring the molecular events controlling the dynamic of the protrusion, we showed that inhibition of the Arp2/3 complex impaired the dynamic of the protrusion by reducing both its maximum length and its growth speed and increasing the delay to start growing. Finally, T cells developed similar protrusions in more physiological conditions, i.e. when activated by an antigen presenting cell (APC) instead of an activating microbead.

Conclusions

Our results suggest that the formation of the force-generating protrusion by T cells is set by an intracellular constant time and that its dynamic is sensitive to external forces. They also show that actin assembly mediated by actin-related protein Arp2/3 complex is involved in the formation and dynamic of the protrusion.

Significance

Actin-rich protrusions developed by T cells are sensory organelles that serve as actuators of immune surveillance. Our study shows that forces experienced by this organelle modify their dynamic suggesting that they might modify immune responses. Moreover, the quantitative aspects of our analysis should help to get insight into the molecular mechanisms involved in the formation of the protrusion.

Introduction

T-cell activation is key in establishing an adaptive immune response and it requires a direct contact between T-cells and antigen presenting cells (APC) where the T-Cell Receptor recognizes the antigenic peptide presented by the major histocompatibility complex MHC. This contact region between both cells forms the immune synapse (IS) and controls several aspects of T cell functions (Dustin and Choudhuri, 2016). We have previously reported that during the IS formation by activation with an antibody-covered microbead mimicking an antigen presenting cell, the T cell produces an actin-rich protrusion. This protrusion generates forces and adapts its growth to the stiffness of the activating surface (Basu et al., 2016; Husson et al., 2011; Sawicka et al., 2017). Seemingly similar protrusions have been observed in T cells contacting another cell, an artificial activating surface, or during transmigration (Cai et al., 2017; Carman et al., 2007; Jung et al., 2016; Sage et al., 2012; Tamzalit et al., 2019; Ueda et al., 2011; Yan et al., 2019). Many questions remain regarding the characteristics of this protrusion. One of them is if and how these force-developing protrusions are modified by forces that are produced by antigen presenting cells such as dendritic cells (Choraghe et al., 2020; Heuzé et al., 2013; Ricart et al., 2011) but also what is the molecular machinery controlling the dynamic of these protrusions. In this report, we further dissect the dynamics of T cell protrusion by exploring the effect of well-defined forces exerted by the cell environment. We also show that the dynamic of the protrusion depends on the ARP2/3 complex. Finally, we observe and characterize the formation of the actin-protrusion in T-cells interacting with an artificial presenting cell model instead of a microbead.

Accepted Article

Results

Description of the setting and characteristic of the activated induced protrusion

We have previously automatized the Micropipette Force Probe (MFP) to apply controlled forces to T lymphocytes (Sawicka et al., 2017; Zak et al., 2019). The MFP uses a flexible micropipette as a cantilever that aspirates an activating microbead. This bead is brought into contact with a leukocyte held by another micropipette. In the present study, we used human primary CD4+ T lymphocytes purified from donor blood and commercial microbeads coated with anti-CD3 + anti-CD28 mAbs known to induce a signaling cascade in T cells and the generation of a protrusion inducing pushing and pulling forces on the activating bead (Husson et al., 2011; Sawicka et al., 2017). The cell-bead contact is ensured by compressing the bead against the cell until a desired force level F_{comp} is reached (Fig. 1A, Suppl. Video 1). It takes few seconds to reach F_{comp}, after which the setup automatically shifts the position of the base of the flexible micropipette to exert a defined force F_{act} on the cell during the rest of the experiments (lasting typically 200 s). F_{act} can be a compressive (F_{act} >0 by convention) or pulling force (F_{act} <0). On top of the level of force F_{act}, the setup superimposes a small oscillatory force of amplitude 0.025-0.050 nN and frequency f = 1 Hz. This force modulation is used to extract the mechanical properties of the cell over time, which evolve during activation, i.e. the lymphocyte becoming stiffer and more viscous during activation (Zak et al., 2019). Here we do not focus on these mechanical changes, but having used the force modulation during our measurements, we checked that the force modulation did not influence the result when F_{act} was comparable to the amplitude of the modulation (Suppl. Mat. 1). Furthermore, experiments were performed at room temperature to limit the thermal drift of the micropipettes. We have shown that at 37°C, T cells react faster than at room temperature, but in a qualitatively comparable manner (Zak et al., 2019). During T cell activation, we measured the cell length, which remained constant for some time after F_{act} was applied. This period is herein called delay (Fig. 1B). This delay ended when the cell started growing a protrusion that was detected by a change in bead position. The growth was first slow, then entered a relatively constant velocity v_{lin}, then slowed down and stopped before switching to a shrinkage phase. We measured v_{lin}, the duration of the growth Δt_{growth}, and the maximal length reached by the protrusion ΔL_{max}, from which we deduced the average growth speed $\langle v \rangle = \Delta L_{max} / \Delta t_{growth}$ (Fig. 1B). v_{lin} was correlated with $\langle v \rangle$ ($v_{lin} \sim 1.4 \langle v \rangle$, see Suppl. Mat. 2), but less variable than $\langle v \rangle$ among cells, so we refer to v_{lin} in this report.

Influence of force on protrusion's delay, length and speed

Because physiologically, T lymphocytes interact with antigen presenting cells (APCs) that might exert some forces on their side, we wondered if the protrusion would be influenced by an external force during activation. To answer this question, we applied the same initial compressive force F_{comp} but varied F_{act}. The influence of F_{act} on the maximum length ΔL_{max} was clear: the higher the compression (F_{act} >0), the shorter the protrusion, and the larger the absolute value of the pulling force (F_{act} <0), the longer the protrusion (Fig. 2A). We further asked if the growing speed v_{lin} was influenced. We observed that compressive forces (F_{act} >0) did not affect v_{lin}. In contrast, v_{lin} significantly increased under pulling force (F_{act}<0) (Fig. 2B). Neither compressive nor pulling forces altered the delay. The average delay for all the F_{act} applied was 38+/-20 s (N=151 cells, n=9 experiments, Fig. 2C). Finally, Δt_{growth} was not influenced by compressive forces but increased under pulling forces (Figure 2D).

This article is protected by copyright. All rights reserved.

Accepted Article

Link between protrusion's diameter and maximal length

Qualitative observations on our data suggested that the diameter of the protrusion depended on its length (Fig. 3A). We thus first quantified the diameter (D_{prot}) of the protrusion at the contact place with the bead at the moment where the protrusion reached its maximal length (ΔL_{max}) for several values of F_{act} (Fig. 3B). We then plotted the maximal length of the protrusion *vs.* its diameter, for all values of F_{act}, and data collapsed on a master curve (Figure 3C), showing that ΔL_{max} and D_{prot} are intimately linked: the longest protrusions were also the thinnest, whatever the level of applied force.

Non-limiting role of membrane stores

We reasoned that this relationship between maximal length and diameter of the protrusion could reflect a physical constraint: the growth of the protrusion could be limited by a maximal amount of membrane stores, which would imply that longer protrusions would be thinner due to limited maximal area. To test this hypothesis, we quantified cell surface area (see methods) at the beginning of the experiments and when the protrusion was the longest. The difference was significant (initial area of 181±25 µm^2 *vs.* largest area of 203±30 µm^2, n=8 experiments, N=76 cells, Fig. 3D) but small: cell surface area was only 12% larger than its initial value. We have shown previously that CD4 T-cells have more than 20% of surface reservoirs in a resting state, and that they can mobilize much larger membrane stores (up to 100% of surface area) during active processes such as transendothelial migration and spreading on an activating surface (Guillou et al., 2016a). Hence, there are large reservoirs available to the T cell beyond 12% area expansion, and limited surface area cannot explain the end of the protrusion's growth. We also considered volume as a physical constraint, but the maximum cell volume was the same as the initial one (maximal volume: 190±58 µm^3; initial volume: 188±72 µm^3, N=44 and 76 cells, respectively, across n=8 experiments, Fig. 3D). Note that the volume of the protrusion starts from zero and increases linearly with time, but represents a small fraction of cell volume. Indeed, when modelled as a cylinder, the volume of the cylindrical protrusion equals its section multiplied by its length. By taking an approximate length of 5 µm and a diameter of about 2 µm, one gets a volume of the protrusion of roughly 16 µm^3, which is only 9 percent of the initial cell volume.

Role of initial compressive force and contact area on protrusion's diameter and maximal length

The master curve in Figure 3C shows that whatever F_{act}, the maximal length ΔL_{max} is determined by D_{prot}, so understanding what sets D_{prot}, can provide an insight on what set the maximal protrusion length ΔL_{max}. We considered the influence of the initial compressive force on D_{prot}, reasoning that this protrusion's diameter, measured just at the moment at which the protrusion stops growing (a moment we call the switch), could be determined by the initial cell-bead contact area. This initial contact area is determined by the level of the initial compression on the cell, F_{comp}: the larger F_{comp}, the larger the initial cell-bead contact. It is difficult to determine this initial contact area from the movies acquired during experiments, but it can be quantified using the Hertz model (Johnson, 1985; Rosenbluth et al., 2006) (see methods and Suppl. Mat. 3) knowing the applied force and the stiffness of the cell. We ran experiments in the simplest case, where F_{act} was set equal to F_{comp}, thus keeping the compression constant during the whole experiment. We expected the protrusion diameter to be equal to the initial contact diameter, and indeed measurement showed an excellent agreement between D_{prot} and the diameter D_{Hertz} predicted by the Hertz model (Fig. 3E). We then asked if the diameter would change if the compression F_{act} was not equal but lower than F_{comp}. The resulting pro-

Accepted Article

trusion diameter D_{prot} was still in excellent agreement with D_{Hertz} set by the initial compressive force. This showed that when the protrusion is kept under compression (F_{act}>0), the protrusion diameter is determined at the stage of the initial cell-bead contact by the level of the initial compressive force F_{comp}. When the protrusion was submitted to a pulling force during its growth (F_{act}<0), two cases could be possible. In a first case, the protrusion diameter could be again determined by the initial compressive force and then remain the same even under pulling force. In the second case, one could expect that the pulling force detaches some bonds at the cell-bead interface, making the protrusion's diameter thinner. To determine which case occurred, we measured the diameter of the protrusion when the initial compression was followed by a small traction force F_{act} = -0.06 nN. This led to the second case mentioned above: the protrusion diameter was smaller than the initial one predicted by the Hertz model (Fig. 3E). This means that the traction forces modulate the protrusion diameter by making it thinner. We hypothesize that this thinning is due to pulling forces ripping off part of the contacts at the cell-bead interface during protrusion's growth. These results strongly suggest that compressive and traction forces exerted by the APCs on the T cells modulate the formation and the dynamic of the protrusion generated by T lymphocytes.

Maximal amount of mobilizable actin in the protrusion

Even though we excluded conservation of cell's total volume as setting the maximal length of the protrusion, the clear trend appearing in the master curve in figure 3C (the longer the protrusion, the thinner), suggested testing if there could be a limitation imposed by a maximal amount of actin available. We reasoned that if available actin in the cell was limiting, each protrusion could stop when all this actin would be stored in the walls of the protrusion. We estimate the volume of actin in the protrusion walls, V_{max}, by multiplying the lateral surface area of the cylindrical protrusion, $S_{lat} = \pi D_{prot} \Delta L_{max}$, with the average thickness of the wall, $e \approx 0.3$ µm. This leads to a prediction that, if the maximal amount of actin is the same in each protrusion when it reaches its maximal length, then ΔL_{max} should be proportional to the inverse of D_{prot}, and proportional to the maximal actin volume, V_{max}: $\Delta L_{max} = \frac{V_{max}}{\pi D_{prot} e}$.

The remaining free parameter, the maximal actin volume V_{max}, could be adjusted by fitting the master curve in figure 3C, leading to V_{max}=7 µm^3. The resulting fit is superimposed to the data in figure 3C. In the discussion, we argue that this can represent a significant part of available actin and that data shown in figure 3C are consistent with a limiting availability of free actin in the cell.

Protrusion length, delay and speed are Arp2/3-dependent, growth duration is not

As shown herein and before, the protrusion is a very dynamic structure. We have previously shown that inhibition of actin polymerization with Latrunculin A treatment abolishes the formation of protrusions by T lymphocytes (Husson et al., 2011). To get more insights into the molecular mechanism supporting the generation by T cells of these protrusions, we asked whether the Arp2/3 complex, which controls nucleation of actin polymerization and branching of filaments, was involved. To do so, we treated cells with the Arp2/3 inhibitor CK666. As opposed to the above-mentioned treatment with Latrunculin A, Arp2/3 inhibition did not abolish the growth of the protrusion. Yet, the effect of CK666 was strong: protrusions reached a lower maximum length (Fig. 4A), started growing later (Fig 4B), with a reduced speed (Fig 4C). In contrast, protrusions growth duration was not significantly altered (Fig. 4D). It is worth mentioning that CK666 treatment did not significantly change cell initial

This article is protected by copyright. All rights reserved.

Accepted Article

stiffness (Suppl. Mat. 4), which might not be intuitive, but is consistent with measurements by others (Fritzsche et al., 2017).

F-actin is enriched in the protrusion, including in a cell-cell system

We have shown before that the protrusion growth is actin-dependent, and that qualitatively, the protrusion appears as an actin cylinder devoid of microtubules (Husson et al., 2011). To further understand how actin is reorganized during the protrusion formation, we focused on the F-actin distribution inside the protrusion. We performed confocal imaging of cells fixed at different timepoints (2, 5, and 10 minutes after introducing cells and beads on a coverslip, see methods). F-actin was depleted in the center of the protrusion (Fig. 5A), recapitulating our observation that the protrusion is a hollow tube formed by F-actin. The protrusion walls were enriched in F-actin when compared to the rest of the cell cortex (Fig. 5C). The enrichment was progressive, starting from the base of the protrusion (see example in Fig. 5A), and the fluorescence intensity reaching a maximal level in the region of the wall in contact with the bead (Fig. 5B), thus forming a thick actin ring reminiscent of what has been observed in 2D studies of the immunological synapse (Cannon and Burkhardt, 2002). Finally, we studied the formation of the actin protrusions in a more physiological model of conjugates formed between T lymphocytes and APC. As model APCs, we used K562 cells expressing the Fc receptor CD64 (named K64, see material and methods) and loaded them with anti-CD3/CD28 activating antibodies like the coated beads used previously. APCs were attached to coverslips. Human CD4+ Jurkat T-cells were then added, and conjugates were fixed after 5 min. The confocal images obtained were very similar to the ones obtained with beads coated with activating mAbs: they showed the formation of protrusion by T cells interacting with activating APC. Moreover, these protrusions showed similar features: a hollow tube enriched in F-actin as compared with the T cell cortex (Fig. 5D-E). These results confirm that when activated by APCs, T cells develop force-generating protrusions that look similar to the protrusions generated when T cells are activated by beads in the MFP setting.

Discussion

Previous works have shown that during the immune synapse formation, T cells produce an actin protrusion that generates forces and adapts its growth to the stiffness of the activating surface (Basu et al., 2016; Husson et al., 2011; Sawicka et al., 2017). The physiological role and the biophysical characteristics of this protrusion remain unknown. In this report, we have applied controlled forces to leukocytes using a Micropipette Force Probe (MFP) to study in detail the behavior of protrusions emitted by T cells following TCR engagement. This method allows getting precise parameters such as the delay required to grow the protrusion, length and diameter of the protrusion, speed of growth and the time at which the protrusion stops growing and retracts (the switch time). Quantifying these parameters can provide valuable information on the molecular mechanisms behind the generation of this protrusion. Our results suggest that the formation of the protrusion is set by an intracellular constant time and that its dynamic is sensitive to external forces. The application of compressive forces slightly decreased the length, duration and velocity of the protrusion formation, whereas pulling forces strongly increase these parameters. We also show that actin assembly mediated by actin-related protein Arp2/3 complex is involved in the formation and dynamic of the protrusion. We ad-

Accepted Article

dressed the relevance of our study in physiological conditions by showing with confocal microscopy that the protrusion is also emitted by T-cells interacting with an artificial antigen presenting cell, suggesting that the protrusion formation is not an artefact due to the bead size or stiffness. Finally, we observed an enrichment of F-actin in the protrusion forming a thick actin ring at the contact with the activating surface, reminiscent of what has been observed in 2D studies of the immunological synapse (Cannon and Burkhardt, 2002).

Similarities exist between the protrusions that we observed and other protrusive structures: T cells were already shown to form protrusive structures that can "invade" the membrane of antigen presenting cells (APC) (Cai et al., 2017; Sage et al., 2012; Ueda et al., 2011). Such protrusions were first described in T lymphocytes during transcellular diapedesis through endothelial cells (Carman et al., 2007) and called invadosome-like protrusions (ILPs). More recently the group of M. Huse also described protrusive structures developed at the immune synapse by cytotoxic T cells that present similarities with ILPs (Tamzalit et al., 2019), i.e. they are enriched in LFA1 and require WASP and Arp2/3 for their formation (Carman et al., 2007). These protrusions are very similar to the protrusions analyzed herein. All these protrusive structures also present similarities with podosomes (and differences, see below), which are dynamic F-actin rich cone-shaped structures (Labernadie et al., 2010), mostly described in myeloid cells. Indeed, podosomes like the protrusions described by others and us are WASP and Arp2/3 dependent for their formation (Kaverina, 2003; Linder et al., 2000). Moreover, podosomes also exert protrusive forces that depend on actin polymerization and increase with the substrate stiffness (Labernadie et al., 2014). Thus, analyses like the one reported herein can provide valuable information on the molecular mechanisms behind the generation of these protrusions.

Concerning the potential role of these structures in T lymphocyte biology, the ILPs by tip toeing on the endothelial cells can help to find the least resistant path for diapedesis (Sage et al., 2012). Protrusive structures, by invading the APC, can also increase the surface of contact between both cells facilitating the binding between ligands and receptors (Ueda et al., 2011). In the case of cytotoxic T cells, protrusions were shown to induce forces responsible for physical deformation and efficient killing of the targets (Basu et al., 2016). Finally, because the protrusions described herein are mechanosensitive, they can sense the stiffness of the APC they interact with (Husson et al., 2011; Sawicka et al., 2017). Since APC stiffness is one of the parameters modulated in inflammatory conditions (Bufi et al., 2015), these protrusive structures may also act as sensory organs to test this parameter and induce an adequate immune response (Saitakis et al., 2017).

The effect of the forces in the dynamic of the protrusion can be compared with the effect of forces on the dynamic of other biological structures. Yet, quantitative data combining both speed and force measurements are scarce in general, including for T cells. For instance, to our knowledge, there are no quantifications of the protrusive force generated by the lamellipodium at the leading edge of migrating T cells. Such lamellipodium, which presents similarities with the protrusions described in this study as it is enriched in branched actin, and its growth is Arp2/3 and WASP dependent, is seen in T cells that migrate at a speed of 0.2-0.5 µm/s (Aoun et al., 2020), quite faster than the ~0.1 µm/s that we measured for T cell protrusions. In macrophage, Labernardie et al. (Labernadie et al., 2014) observed periodic protrusions of podosomes of 20 nm with a typical period of 40 s, hence a typical growth speed of 0.5 nm/s, two orders of magnitude slower than T cell protrusions. However, these observations were done for macrophages adhering on a substrate. Even

This article is protected by copyright. All rights reserved.

Accepted Article

considering that, without a resisting substrate, podosome could grow up to ~600nm in height as observed previously by Labernadie et al. (Labernadie et al., 2010) with a comparable timescale would lead to a growth typically ten times slower than T cell protrusions, suggesting that podosomes are not similar to T cell protrusions. Considering further quantitative data of both force and velocity in cell structures, Prass *et al.* (Prass et al., 2006) have quantified the force generated by the lamellipodium of a fish keratocyte migrating against an atomic force microscope (AFM) cantilever. They measured a growth velocity under no force of ~0.02 µm/s, which is much lower than the growing speed of about 0.11 µm/s that we measured for T cell protrusions. We can also compare the influence of force on growth speed. To perform this comparison, the surface over which the compressive force is applied has to be taken into account, to compare stresses (force per surface area) instead of forces. For a T cell protrusion, we assume that the surface of the actin cortex supporting the stress is the section of a cylinder of diameter D_{prot}, thickness e ~ 0.3 µm (Chugh et al., 2017), and surface area $\pi D_{prot} e$. The resulting stress is $\sigma = F_{act}/(\pi D_{prot} e)$, and numerically, for a compressive force F_{act} = 0.36 nN, we get a compressive stress of ~390 Pa. In the setup used by Prass *et al.* (Prass et al., 2006), the cantilever contacts the lamellipodium over a surface of about 3µm x 0.2µm = 0.6 μm^2. Interestingly, the authors see barely any reduction of the growth speed at a force of up to about 0.6 nN, translating into a stress of about 1 kPa. This is consistent with our measurements, as we measured almost no reduction in speed up to an applied stress of 390 Pa. This means that T cells protrusion are much faster than a lamellipodium, but display the same insensitivity to compressive stresses as the lamellipodium of a keratocyte.

The dynamics of the T cell protrusions can also be compared to that of reconstituted actin gels, for which a wide range of growth velocity has been measured. When growing against an AFM cantilever, Bieling *et al.* measured a velocity of about 0.12 µm/s under no force, very close to our observations on protrusions (Bieling et al., 2016). However, in a previous study with a similar setup but different molecular components, Parekh et al. measured a much lower speed in the range of 0.001-0.01 µm/s (Parekh et al., 2005). The latter velocity range matches the one obtained by Baüer *et al.* in actin gels growing against magnetic colloids (Bauër et al., 2017), while Marcy *et al.* found an intermediate value of ~0.03 µm/s for actin comets growing against a microfiber (Marcy et al., 2004). Next, to compare the influence of forces to the growing speed of actin comets (Marcy et al., 2004), we assume the latter to be actin-filled cylinders of diameter $D_{comet} \approx 2$ µm, hence a section of surface area $\pi D^2_{comet}/4$, leading to stress $\sigma = F/(\pi D^2_{comet}/4)$ under a force F. Under a tensile stress of 130 Pa, Marcy *et al.* find an increase in the comet velocity of only 10% compared to free growth, while we found an increase of about 50% in protrusions under the same tensile stress. Moreover, under a compressive stress of ~390 Pa, as stated above, we see a weak effect of the force on the growing speed, while Marcy *et al.* see a 30-40% decrease in growth velocity. In the case of gels grown against a cantilever, the decrease due to compressive force is much larger, gels are up to four folds slower than free growth under a ~390-Pa compressive stress (Bauër et al., 2017; Bieling et al., 2016). Thus, T cell protrusions are as fast as the faster growing gels, when compared to actin comets, protrusions are more sensitive to tensile stress and less sensitive to compressive stress. Gels grown against a cantilever are even more sensitive to compressive force. We conclude – maybe unsurprisingly – that the cell protrusions have different mechanical dynamics than reconstituted systems. Consistent with this, Bieling *et al.* showed that the presence of the Arp2/3 complex has a large influence on gel mechanical behavior as opposed to random, isotropic crosslinked actin networks. In cells, where in addition to the Arp2/3 complex, many molecules, including filamin-A (Flanagan et al., 2001), α-actinin,

Accepted Article

filamin (Esue et al., 2009), and other capping and branching factors (Pujol et al., 2012) are present to regulate the cortex assembly, we expect even more "exotic" behavior of the cellular actin cortex. To further our understanding at the cell level, we plan to implement simultaneous force and fluorescence measurements to study how 3D actin flows are structured within the protrusion, possibly similar to flows during T cell migration and swimming (Aoun et al., 2020; Reversat et al., 2020). Furthermore, as in vitro studies have shown that actin dynamics depend on the level of external compressive forces (Bieling et al., 2016) and that actin waves can be triggered in cells under external forces (Kapustina et al., 2013), it might also be interesting in the future to study actin dynamics under different levels of compressive forces in T cells during their activation.

Our results also show that external forces differentially affect the duration of the protrusion growth (switch time). This switch seems to be set by an intracellular "clock" and its origin is yet not clear since we identified its existence in a previous study (Husson et al., 2011). Here we observed that when a compressive force is applied, the duration of the growth and the delay barely depend on the amplitude of the compressive force. In our previous study using a different micropipette-based technique (a biomembrane force probe) (Husson et al., 2011), we measured a delay time of 45+/-7 s remarkably close to the one measured in this study. We measured a growth duration that was 140+/-15 s, *vs.* 50-90 s in this study (Husson et al., 2011). Although the setup we used previously presented several differences, an important one is that the setup was not automated to apply a controlled force to the growing protrusion, and pulling forces applied to the growing protrusion were possibly relatively large. As we showed that the larger the amplitude of the pulling force, the longer the growth duration, this can explain why we found a longer growth duration in our previous study. When pulling force is exerted, the stronger the force, the longer the growth duration. Pulling forces are expected to help to unfold the surface membrane stores, hence allowing the protrusion to grow longer. We hypothesize that the switch time could depend on a limitation of these membrane stores unfolded by pulling forces. However, we excluded that the switch time was defined by limited membrane store by showing that the surface area expansion of the cell during activation is much lower than membrane reservoirs of CD4 T cells. We have previously quantified the membrane stores that these cells can mobilize during different active processes such as transendothelial migration or spreading on an activating surface (Guillou et al. 2016).

Finally, we asked if the switch could be explained by the exhaustion of mobilizable stocks of actin to grow the protrusion. Inhibiting the Arp2/3 complex did not change the switch time, but increased the delay before growth. This showed that branched actin is necessary to build the protrusion, but that the switch does not depend on actin branching. This seems not easy to reconcile with a limiting amount of available actin setting the maximal length of the protrusion, except if the shorter protrusions observed in the presence of CK666 are much wider so that they contain as much actin as in untreated cells. Unfortunately, measuring the protrusion diameter of such a small protrusion is very difficult on the videos and we could not assess that. We estimated that the geometry of the protrusion when it reached its maximal length was consistent with a conserved maximal amount of actin contained in the protrusion of about 7 μm^3. This volume can be compared to the total amount of actin in the cell. We estimate a cortex thickness of 0.2 µm in a resting primary T cell with an average diameter of 6.7 µm (Guillou et al., 2016a). We obtain a volume of actin contained in the cortex of about 30 μm^3. Considering that the enrichment in actin in the protrusion relative to the cortex outside the protrusion leads to an increase in density of a factor of about three (as deduced from the increase in fluorescence intensity that we measured, Fig. 5), the protrusion could represent up to

This article is protected by copyright. All rights reserved.

Accepted Article

two thirds of the initial amount of actin present in the cortex of the resting cell. The fact that there seems to be a maximal amount of actin in the protrusion, and that it represents a significant percentage of the total amount of available actin suggests that the amount of available actin can be a factor that defines the switch. We will consider testing in the future the limited actin hypothesis, one possibility being to use recently developed photo-activable actin-associated inhibitors (Borowiak et al., 2020).

In conclusion, our study suggests that the switch and the delay are set by an intracellular constant time and that the maximal length of the protrusion is set by a constant growth speed. Our study provides key insights that help to better understand the mechanism involved in the formation of the actin protrusion emitted by the T-cell, a process at the core of T cell activation.

Materials and Methods

Micropipette Force Probe

The Micropipette Force Probe is a micropipette-based assay using a flexible micropipette as a cantilever (Sawicka et al., 2017). The flexible micropipette aspirates a bead covered with antibodies at its tip. In this study beads were Dynabeads® Human T-Activator CD3/CD28 for T Cell Expansion and Activation from Gibco, purchased from Thermo Fisher Scientific (ref. 11131D, Carlsbad, CA). Micropipettes were prepared as described elsewhere (Basu et al., 2016; Guillou et al., 2016b, 2016a; Sawicka et al., 2017) using borosilicate glass capillaries (Harvard Apparatus, Holliston, MA, USA) with a micropipette puller (P-97, Sutter Instruments, Novato, CA, USA), cutting them with a microforge (MF-200, World Precision Instruments, Sarasota, FL, USA) and bending them at a 45° angle with another microforge (MF-900, Narishige, Tokyo, Japan). Micropipettes were held by micropipette holders (IM-H1, Narishige) placed at a 45° angle relative to the plane of the microscope stage, so that micropipette tips were in the focal plane of an inverted microscope under brightfield or DIC illumination (Ti2, Nikon Instruments, Tokyo, Japan) equipped with a 100× oil immersion, 1.3 NA objective (Nikon Instruments) and placed on an air suspension table (Newport). The flexible micropipette was linked to a micropositioner (Thorlabs, Newton, NJ, USA) placed on top of a single-axis stage controlled with a closed loop piezo actuator (TPZ001; Thorlabs). The bending stiffness k of the flexible micropipette (about 0.1-0.3 nN/µm) was measured against a standard microindenter calibrated with a commercial force probe (model 406A; Aurora Scientific, Aurora, ON, Canada). Experiments were performed in glass-bottom Petri dishes (Fluorodish, WPI, Sarasota, FL, USA). Once an activating microbead was aspirated by the flexible micropipette, a T cell was picked up at the bottom of the Petri dish, held by a stiff micropipette with an aspiration pressure of 30-60 Pa (imposed by lowering the water level in a reservoir connected to the micropipette), and brought in adequate position using a motorized micromanipulator (MP-285; Sutter Instruments). This aspiration pressure is necessary to hold the cell to prepare and during experiments. In a previous study we showed that below and expansion of the cell membrane area of a resting T cell of about 20%, the mechanical properties of cell is not affected. Below this threshold, cell surface area expansion leads to an increase in cell effective stiffness that could potentially affect cell response (Guillou et al., 2016a), but we did not exceed this 20% threshold Images were acquired using a Flash 4.0 or ORCA-spark CMOS camera (Hamamatsu Photonics, Hamamatsu City, Japan). The setup automatically detects the position of the bead at the tip of the force probe at a rate of about 400 and imposes the position of the base of the flexible micropipette by controlling the position of the piezo stage. The deflection of the force probe is the

Accepted Article

difference between the position of the bead and the position of the piezo stage. Thus, the force applied to the cell is the product of this deflection by the bending stiffness *k*. A retroaction implemented in Matlab (Mathworks) controlling both the camera via the Micromanager software (Edelstein et al., 2014) and the piezo stage moves the latter in reaction to the measurement of the bead position in order to keep a desired deflection of the cantilever, so that a defined force is applied to the cell at any given time. Experiments were performed at room temperature to avoid thermal drift.

Cells

Mononuclear cells were isolated from peripheral blood of healthy donors on a ficoll density gradient. Buffy coats from healthy donors (both male and female donors) were obtained from Etablissement Français du Sang (Paris, France) in accordance with INSERM ethical guidelines. Human total CD4+ isolation kit (Miltenyi Biotech, 130-096-533) was used for the purification of T cells. Arp2/3 inhibition (Fig. 4) was performed with a 30-min preincubation with CK666 (25µM), which was left in the extracellular medium during experiments. DMSO content in control was 0.1% V/V.

K562 CCL-243 ATCC transduced with lentiviral particles encoding for CD64 (named K64 cells) were cultured at 37 °C 5% CO2 in RPMI 1640 Glutamax (Gibco, 61870-010) supplemented with 10% fetal calf serum (FCS, Corning, 35-079-CV, lot no. 35079011) and were passed every 2–3 days at ~0.5×10^6 cells/mL.

Production of lentiviruses and infection of K562 cells.

Non-replicative VSV-g pseudotyped lentiviral particles were produced by transfecting HEK-293T cells with Gag, Pol, rev, encoding plasmid (pPAX2), envelop encoding plasmid (pMD2.G) and the CD64 construct (Provided by Philipe Bernaroch) encoded in a pWXLD vector. Lentivirus were recovered in supernatant after 2 days and concentrated. 5×10^6 K562 cells were infected for 24 h, and used 3-5 days post infection.

Coverslips and dishes preparation for immunofluorescence assay

12mm ø coverslips (VWR, 631-0666) for fixed cells were pre-coated with 0.02% of poly-L-Lysine (Sigma Aldrich P8920) for 20 min at room temperature and were washed three times in water before being dried and kept for maximum of 2 days.

Preparation of CD4+ and CD3/CD28 Beads conjugates

CD4+ T cells cells were resuspended at 2×10^6 in 1 mL of RPMI medium. An equal volume of magnetic beads (2×10^6) coated with anti-CD3 and anti-CD28 (Gibco, 11132D) was added. The Cells-Beads mix was incubated on a coverslip for the appropriate time (2, 5 and 10 min) at 37 °C. Coverslips were then washed once with cold PBS before fixation.

Preparation of primary CD4-T cells and K64 cells conjugates

K64 cells were washed, resuspended at a concentration of 1×10^6 cells/mL, then loaded with anti CD3 (OKT3 clone, eBioscience, 16-0037-85, 10 µg/mL final concentration) and anti-CD28 (LEAF Purified anti-human CD28 from CD28.2 clone, Biolegend, BLE302923 at 10 µg/mL final concentration) for 30 min at 37 °C before being washed once and resuspended at a concentration of 1×10^6 cells/mL. 150,000 K64 cells were incubated on coverslips for 30 min, washed once with warmed PBS and 250,000 CD4 T cells resuspended in RPMI 10% FCS were added for 5 min. Coverslips were washed once with cold PBS before fixation.

This article is protected by copyright. All rights reserved.

Accepted Article

Fixation

Cells were fixed with 4% paraformaldehyde (Life technologies, FB002) for 15 min at room temperature, washed once in PBS and excess of paraformaldehyde was quenched for 10 min with PBS 10 mM Glycine (Thermo Fisher Scientific, G8898). Coverslips were kept at 4 °C in PBS until permeabilization and staining.

Staining and mounting

Cells were permeabilized for 30 min at room temperature with PBS 0.2% Bovine Serum Albumin (BSA, Euromedex, 04-100-812) 0.05% Saponin (Sigma-Aldrich, S4521). Cells were then incubated at room temperature for 30 min in the same buffer with Alexa Fluor 647 phalloidin (Invitrogen A22287). After washing once with PBS BSA Saponin, and once with PBS, coverslips were soaked three times in PBS, three times in water, and mounted with 4–6 µL of Fluoromount G (SouthernBiotech, 0100-01) on slides (KNITTEL Starfrost) and dried overnight protected from light before microscope acquisition.

Confocal microscopy and image analysis

Images were acquired with a Leica DmI8 inverted microscope equipped with an SP8 confocal unit using either a 40X (1.35NA) or 63X (1.4NA) objective. Single plane images or Z-stack of images were acquired. Images were analyzed on Fiji and ImageJ software using scripts generated for automated or semi-automated analysis.

Hertz model

The Hertz model (Johnson, 1985; Rosenbluth et al., 2006) applies to the deformation of an elastic medium when indented by a sphere. The model can be extended in the case of the indentation of an elastic sphere (representing the cell) by an infinitely stiff spherical indenter (representing the microbead), which leads to the following relationship between the compressive force *F* applied by the indenter on the elastic sphere and indentation δ of the latter: $F = \frac{4}{3}\frac{E_{Young}}{1-\nu^2}\sqrt{R_{eff}}\delta^{\frac{3}{2}}$, where E_{Young} is the effective Young's modulus of the cell, R_{eff} is an effective radius given by $1/R_{eff} = 1/R_{cell} + 1/R_{bead}$, with R_{cell} the cells radius and R_{bead} the bead radius, ν is the Poisson ratio of the cell taken as 0.5 (i.e. the cell is considered incompressible (Moeendarbary et al., 2013; Wu et al., 2018).

We first used this model during the initial indentation of T cells by the activating microbead. During an experiment, the base of the flexible pipette holding the bead is translated at a constant velocity towards the cell. Upon contact, the bead starts applying an increasing compressible force to the cell, until it reaches the force level $F_{comp.}$ During this initial compressive phase, we measured both applied force and cell indentation. We fitted the experimental *F*-δ curve using the above *F*-δ relationship (Suppl. Mat. 3).

Furthermore, the Hertz model predicts that the radius *a* of the cell-bead contact area is such that $a^2 = R_{eff}\delta$. By substituting a in the *F*-δ relationship above, we get: $F = \frac{4}{3}\frac{E_{Young}}{1-\nu^2}\frac{a^3}{R_{eff}}$, hence *a* can be calculated knowing cell properties and applied force by inverting the previous relationship, leading to: $a = \left(\frac{FR_{eff}}{\frac{4E_{Young}}{3\ 1-\nu^2}}\right)^{1/3}$.

Accepted Article

Volume and surface area calculation

The surface and volume of the cells were calculated assuming an axisymmetrical geometry of the cell around the axis defined by the cell center and bead center (horizontal axis in Suppl. Video 1). The contour of cells was hand-traced using image j software (Schneider et al., 2012) using a segmented line, thus defining small cylinders of diameter equal to the local cell diameter and of small (submicron) thickness. Once sliced in elementary cylinders, the lateral area or volume of these cylinders is readily computed. The sum leads to the desired cell surface area and volume.

References

Aoun, L., Farutin, A., Garcia-Seyda, N., Nègre, P., Rizvi, M.S., Tlili, S., Song, S., Luo, X., Biarnes-Pelicot, M., Galland, R., et al. (2020). Amoeboid Swimming Is Propelled by Molecular Paddling in Lymphocytes. Biophys. J. *119*, 1157–1177.

Basu, R., Whitlock, B.M.B.M., Husson, J., Le Floc'h, A., Jin, W., Oyler-Yaniv, A., Dotiwala, F., Giannone, G., Hivroz, C., Biais, N., et al. (2016). Cytotoxic T Cells Use Mechanical Force to Potentiate Target Cell Killing. Cell *165*, 100–110.

Bauër, P., Tavacoli, J., Pujol, T., Planade, J., Heuvingh, J., and Du Roure, O. (2017). A new method to measure mechanics and dynamic assembly of branched actin networks. Sci. Rep. *7*, 15688.

Bieling, P., Li, T. De, Weichsel, J., McGorty, R., Jreij, P., Huang, B., Fletcher, D.A., and Mullins, R.D. (2016). Force Feedback Controls Motor Activity and Mechanical Properties of Self-Assembling Branched Actin Networks. Cell *164*, 115–127.

Borowiak, M., Küllmer, F., Gegenfurtner, F., Peil, S., Nasufovic, V., Zahler, S., Thorn-Seshold, O., Trauner, D., and Arndt, H.D. (2020). Optical Manipulation of F-Actin with Photoswitchable Small Molecules. J. Am. Chem. Soc.

Bufi, N., Saitakis, M., Dogniaux, S., Buschinger, O., Bohineust, A., Richert, A., Maurin, M., Hivroz, C., and Asnacios, A. (2015). Human primary immune cells exhibit distinct mechanical properties that are modified by inflammation. Biophys. J. *108*, 2181–2190.

Cai, E., Marchuk, K., Beemiller, P., Beppler, C., Rubashkin, M.G., Weaver, V.M., Gérard, A., Liu, T.L., Chen, B.C., Betzig, E., et al. (2017). Visualizing dynamic microvillar search and stabilization during ligand detection by T cells. Science (80-.). *356*.

Cannon, J.L., and Burkhardt, J.K. (2002). The regulation of actin remodeling during T-cell-APC conjugate formation. Immunol. Rev. *186*, 90–99.

Carman, C., Sage, P., and Sciuto, T. (2007). Transcellular diapedesis is initiated by invasive podosomes. Immunity *26*, 784–797.

Choraghe, R.P., Kołodziej, T., Buser, A., Rajfur, Z., and Neumann, A.K. (2020). RHOA-mediated mechanical force generation through Dectin-1. J. Cell Sci.

Chugh, P., Clark, A.G., Smith, M.B., Cassani, D.A.D., Dierkes, K., Ragab, A., Roux, P.P., Charras, G., Salbreux, G., and Paluch, E.K. (2017). Actin cortex architecture regulates cell surface tension. Nat.

This article is protected by copyright. All rights reserved.

Accepted Article

Cell Biol. *19*, 689–697.

Dustin, M.L., and Choudhuri, K. (2016). Signaling and Polarized Communication Across the T Cell Immunological Synapse. Annu. Rev. Cell Dev. Biol. *32*, 303–325.

Edelstein, A.D., Tsuchida, M. a, Amodaj, N., Pinkard, H., Vale, R.D., and Stuurman, N. (2014). Advanced methods of microscope control using μManager software. J. Biol. Methods *1*, 10.

Esue, O., Tseng, Y., and Wirtz, D. (2009). A-Actinin and Filamin Cooperatively Enhance the Stiffness of Actin Filament Networks. PLoS One *4*, 1–6.

Flanagan, L.A., Chou, J., Falet, H., Neujahr, R., Hartwig, J.H., and Stossel, T.P. (2001). Filamin A, the Arp2/3 complex, and the morphology and function of cortical actin filaments in human melanoma cells. J. Cell Biol. *155*, 511–518.

Fritzsche, M., Li, D., Colin-York, H., Chang, V.T., Moeendarbary, E., Felce, J.H., Sezgin, E., Charras, G., Betzig, E., and Eggeling, C. (2017). Self-organizing actin patterns shape membrane architecture but not cell mechanics. Nat. Commun. *8*, 17–19.

Guillou, L., Babataheri, A., Saitakis, M., Bohineust, A., Dogniaux, S., Hivroz, C., Barakat, A.I., and Husson, J. (2016a). T-lymphocyte passive deformation is controlled by unfolding of membrane surface reservoirs. Mol. Biol. Cell *27*, 3574–3582.

Guillou, L., Babataheri, A., Puech, P.-H., Barakat, A.I., and Husson, J. (2016b). Dynamic monitoring of cell mechanical properties using profile microindentation. Sci. Rep. *6*, 21529.

Heuzé, M.L., Vargas, P., Chabaud, M., Le Berre, M., Liu, Y.J., Collin, O., Solanes, P., Voituriez, R., Piel, M., and Lennon-Duménil, A.M. (2013). Migration of dendritic cells: Physical principles, molecular mechanisms, and functional implications. Immunol. Rev.

Husson, J., Chemin, K., Bohineust, A., Hivroz, C., and Henry, N. (2011). Force Generation upon T Cell Receptor Engagement. PLoS One *6*, e19680.

Johnson, K.L. (1985). Contact Mechanics. J. Am. Chem. Soc. *37*, 1–17.

Jung, Y., Riven, I., Feigelson, S.W., Kartvelishvily, E., Tohya, K., Miyasaka, M., Alon, R., and Haran, G. (2016). Three-dimensional localization of T-cell receptors in relation to microvilli using a combination of superresolution microscopies. Proc. Natl. Acad. Sci. *113*, E5916–E5924.

Kapustina, M., Elston, T.C., and Jacobson, K. (2013). Compression and dilation of the membrane-cortex layer generates rapid changes in cell shape. J. Cell Biol. *200*, 95–108.

Kaverina, I. (2003). Podosome formation in cultured A7r5 vascular smooth muscle cells requires Arp2/3-dependent de-novo actin polymerization at discrete microdomains. J. Cell Sci. *116*, 4915–4924.

Labernadie, A., Thibault, C., Vieu, C., Maridonneau-Parini, I., and Charriere, G.M. (2010). Dynamics of podosome stiffness revealed by atomic force microscopy. Proc. Natl. Acad. Sci. *107*, 21016–21021.

Labernadie, A., Bouissou, A., Delobelle, P., Balor, S., Voituriez, R., Proag, A., Fourquaux, I., Thibault, C., Vieu, C., Poincloux, R., et al. (2014). Protrusion force microscopy reveals oscillatory force generation and mechanosensing activity of human macrophage podosomes. Nat. Commun. *5*, 5343.

Linder, S., Higgs, H., Hüfner, K., Schwarz, K., Pannicke, U., and Aepfelbacher, M. (2000). The Polarization Defect of Wiskott-Aldrich Syndrome Macrophages Is Linked to Dislocalization of the Arp2/3 Complex. J. Immunol. *165*, 221–225.

Accepted Article

Marcy, Y., Prost, J., Carlier, M.-F., and Sykes, C. (2004). Forces generated during actin-based propulsion: a direct measurement by micromanipulation. Proc. Natl. Acad. Sci. U. S. A. *101*, 5992–5997.

Moeendarbary, E., Valon, L., Fritzsche, M., Harris, A.R., Moulding, D.A., Thrasher, A.J., Stride, E., Mahadevan, L., and Charras, G.T. (2013). The cytoplasm of living cells behaves as a poroelastic material. Nat. Mater. *12*, 253–261.

Parekh, S.H., Chaudhuri, O., Theriot, J.A., and Fletcher, D.A. (2005). Loading history determines the velocity of actin-network growth. Nat. Cell Biol. *7*, 1119–1123.

Prass, M., Jacobson, K., Mogilner, A., and Radmacher, M. (2006). Direct measurement of the lamellipodial protrusive force in a migrating cell. J. Cell Biol. *174*, 767–772.

Pujol, T., Du Roure, O., Fermigier, M., and Heuvingh, J. (2012). Impact of branching on the elasticity of actin networks. Proc. Natl. Acad. Sci. U. S. A. *109*, 10364–10369.

Reversat, A., Gaertner, F., Merrin, J., Stopp, J., Tasciyan, S., Aguilera, J., de Vries, I., Hauschild, R., Hons, M., Piel, M., et al. (2020). Cellular locomotion using environmental topography. Nature.

Ricart, B.G., Yang, M.T., Hunter, C.A., Chen, C.S., and Hammer, D.A. (2011). Measuring traction forces of motile dendritic cells on micropost arrays. Biophys. J.

Rosenbluth, M.J., Lam, W.A., and Fletcher, D.A. (2006). Force microscopy of nonadherent cells: a comparison of leukemia cell deformability. Biophys. J. *90*, 2994–3003.

Sage, P.T., Varghese, L.M., Martinelli, R., Sciuto, T.E., Kamei, M., Dvorak, A.M., Springer, T.A., Sharpe, A.H., and Carman, C. V. (2012). Antigen Recognition Is Facilitated by Invadosome-like Protrusions Formed by Memory/Effector T Cells. J. Immunol. *188*, 3686–3699.

Saitakis, M., Dogniaux, S., Goudot, C., Bufi, N., Asnacios, S., Maurin, M., Randriamampita, C., Asnacios, A., and Hivroz, C. (2017). Different TCR-induced T lymphocyte responses are potentiated by stiffness with variable sensitivity. Elife *6*, 1–29.

Sawicka, A., Babataheri, A., Dogniaux, S., Barakat, A.I., Gonzalez-Rodriguez, D., Hivroz, C., and Husson, J. (2017). Micropipette Force Probe to quantify single-cell force generation: application to T cell activation. Mol. Biol. Cell *28*, mbc.E17-06-0385.

Schneider, C. a, Rasband, W.S., and Eliceiri, K.W. (2012). NIH Image to ImageJ: 25 years of image analysis. Nat. Methods *9*, 671–675.

Tamzalit, F., Wang, M.S., Jin, W., Tello-Lafoz, M., Boyko, V., Heddleston, J.M., Black, C.T., Kam, L.C., and Huse, M. (2019). Interfacial actin protrusions mechanically enhance killing by cytotoxic T cells. Sci. Immunol. *4*, eaav5445.

Ueda, H., Morphew, M.K., McIntosh, J.R., and Davis, M.M. (2011). CD4+ T-cell synapses involve multiple distinct stages. Proc. Natl. Acad. Sci. U. S. A. *108*, 17099–17104.

Wu, P.-H., Aroush, D.R.-B., Asnacios, A., Chen, W.-C., Dokukin, M.E., Doss, B.L., Durand-Smet, P., Ekpenyong, A., Guck, J., Guz, N. V., et al. (2018). A comparison of methods to assess cell mechanical properties. Nat. Methods *15*, 491–498.

Yan, S.L.S., Hwang, I.Y., Kamenyeva, O., and Kehrl, J.H. (2019). In Vivo F-Actin Filament Organization during Lymphocyte Transendothelial and Interstitial Migration Revealed by Intravital Microscopy. IScience *16*, 283–297.

This article is protected by copyright. All rights reserved.

Accepted Article

Zak, A., Violeta, S., Cortés, M., Sadoun, A., Babataheri, A., Dogniaux, S., Dupré-crochet, S., Hudik, E., He, H., Barakat, A.I., et al. (2019). Single-cell immuno-mechanics : rapid viscoelastic changes are a hall- mark of early leukocyte activation. Bioarxiv.

Acknowledgements

J.H. thanks M.E. Serrentino and E. Husson for fruitful discussion and J. Heuvingh for insight on in vitro actin dynamics. J.H. tanks the LadHyX members for technical support. This work has benefited from the financial support of the LabeX LaSIPS (ANR-10-LABX-0040-LaSIPS) managed by the French National Research Agency under the “Investissements d’avenir”program (ANR-11-IDEX-0003-02). This work was also supported by Ecole polytechnique, a CNRS PEPS funding, and an endowment in cardiovascular cellular engineering from the AXA Research Fund. For her salary, N.P. benefits of the financial support from ITMO Cancer Aviesan (Alliance Nationale pour les Sciences de la Vie et de la Santé/ National Alliance for Life Sciences & Health) within the framework of the Cancer Plan (ED 474 /ITMO Cancer Aviesan partnership). The project "Mechanical probing of tumor infiltrating lympho-cytes" benefits from a funding by the Bettencourt Schueller Foundation.

Author Contribution

A.E.Z. designed, performed and quantified the confocal microscopy experiments and contributed to writing the manuscript. N.P. set up the K64 cells as artificial APC. S.D. prepared shRNA lentivirus and purified plasmids encoding chimeric molecules. O. M. designed and realized the graphical abstract and contributed to writing the manuscript, C.H. provided key material, discussed the results and contributed to writing the manuscript. J.H. designed, performed and analyzed all the MFP experi-ments, analyzed the confocal images, conceived the study and wrote the manuscript.

Accepted Article

Figure Legends

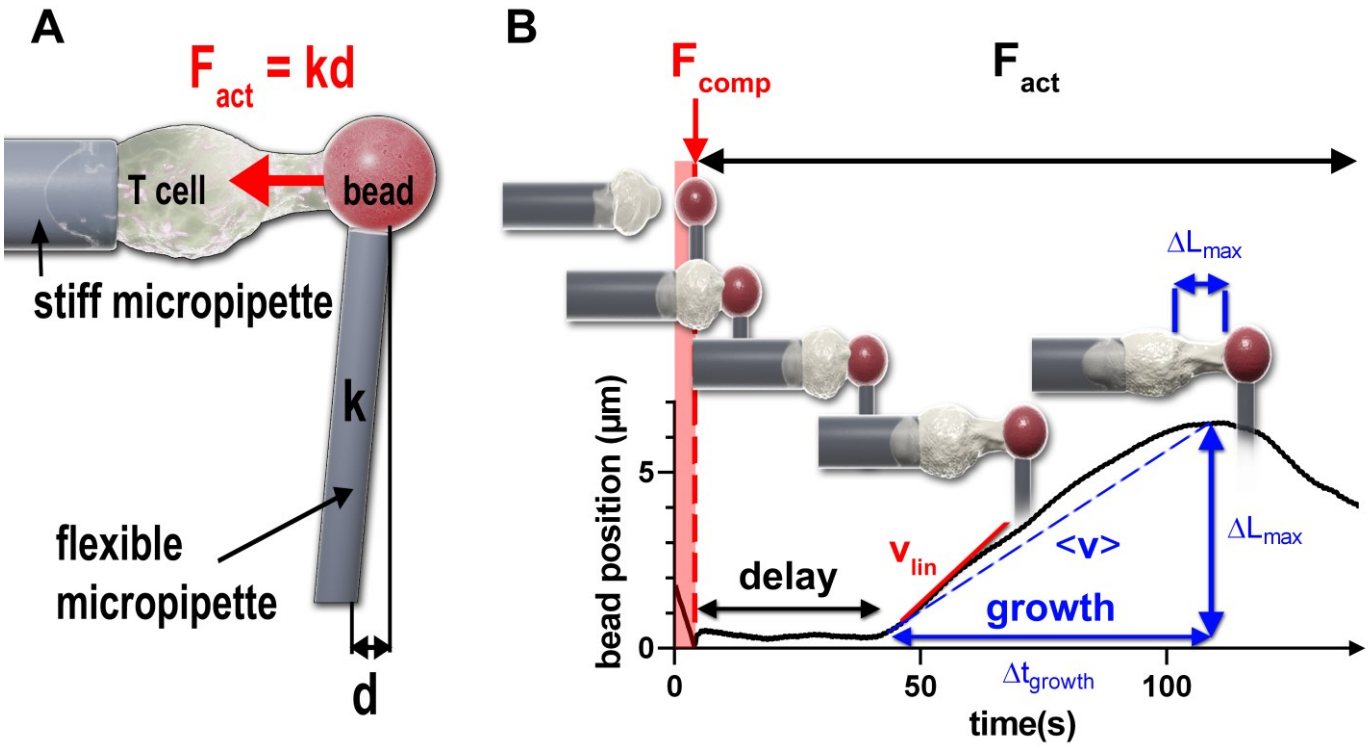

Figure 1. A. Micropipette Force Probe (MFP). A stiff micropipette holds a T cell. A flexible micropipette of bending stiffness *k* aspirates firmly an activating microbead. The deflexion *d* of the micropipette (not to scale) is controlled to apply the desired force level during cell activation, $F_{act} = k \times d$. B. Representative curve of the bead position (measuring cell length) *vs* time. The maximal protrusion length is ΔL_{max}. The initial cell-bead contact is ensured by applying an initial compressive force F_{comp}, after which an average force F_{act} is applied during the rest of the experiment (with an added small force modulation to perform other mechanical measurements, see text).

This article is protected by copyright. All rights reserved.

Accepted Article

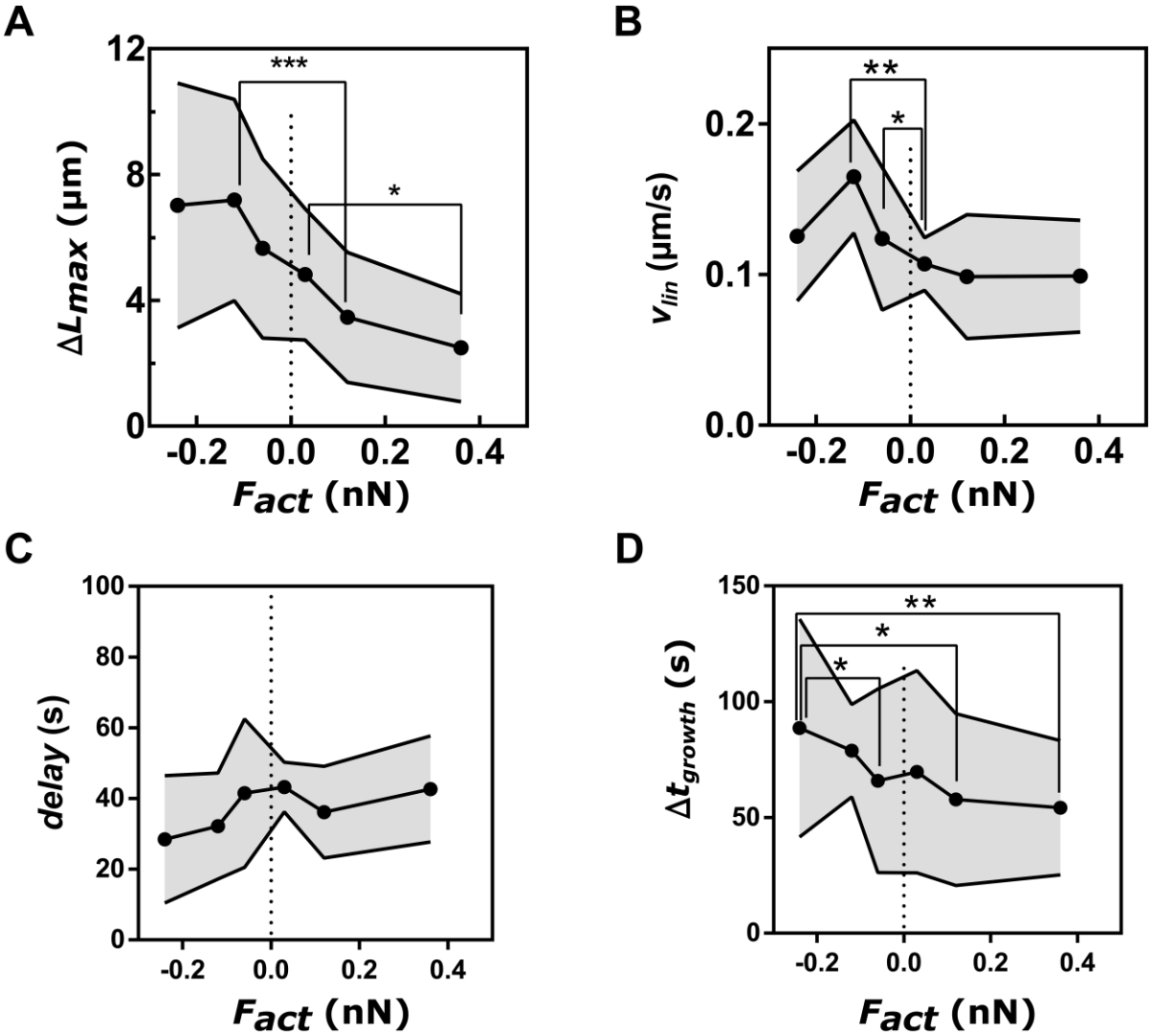

Figure 2. Influence of the applied force during activation F_{act} on several parameters (all cells were submitted to F_{comp}=0.36 nN). A. Maximal protrusion length ΔL_{max}. B. Growth speed v_{lin}. C. Delay. D. Growth duration Δt_{growth}. Data in A-D represent 8 experiments, each dot is an average over 7 to 20 cells, except in B where the average is over 3 to 17 cells. Gray area represents SDs. Statistical tests: two-tailed t-test with Welch's correction (* p<0.05; ** p<0.01; *** p<0.001).

Accepted Article

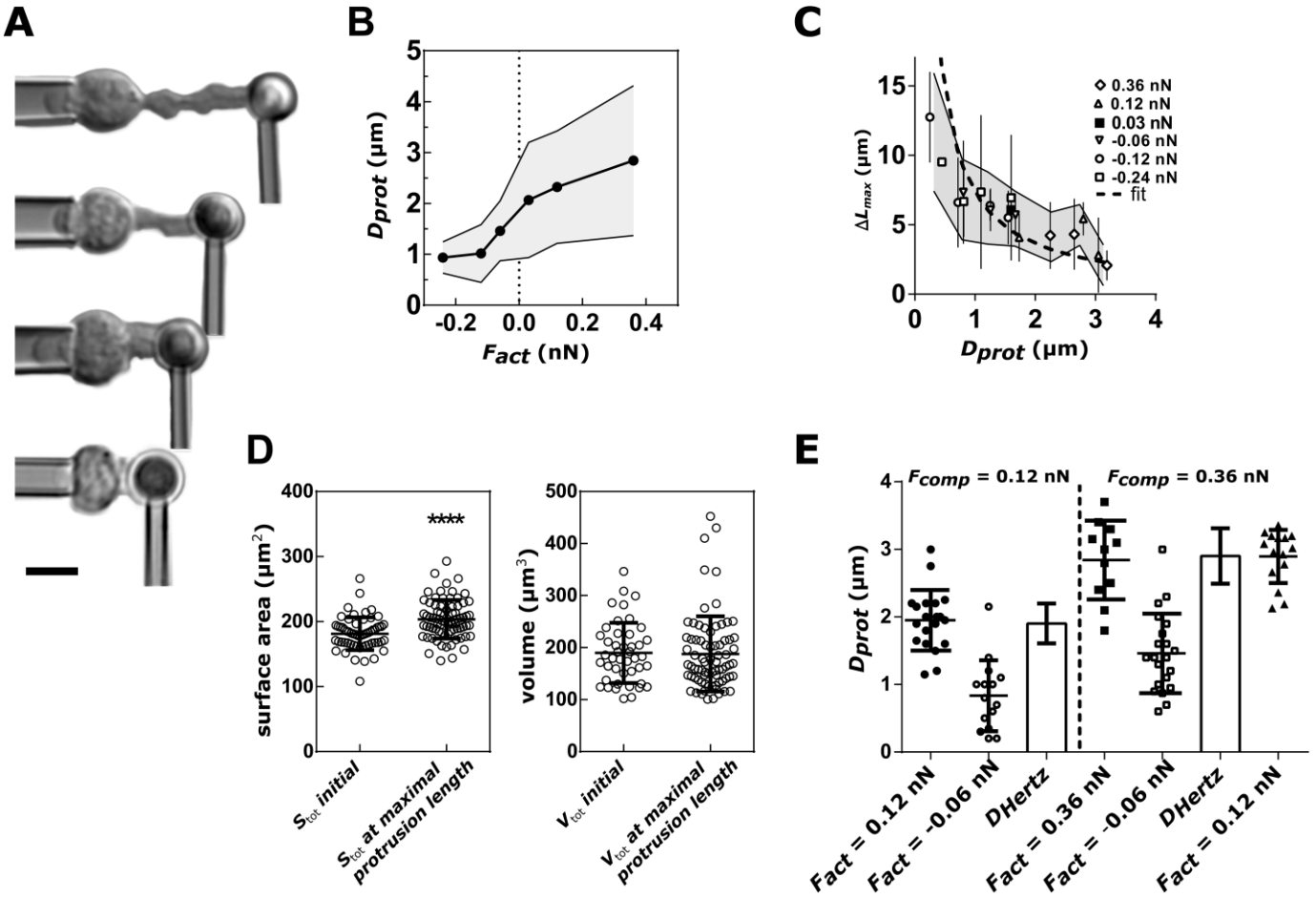

Figure 3. A. Images of the Micropipette Force Probe (images denoised, contrasted, and the background was removed, bar: 5 µm). Cells were submitted to increasing level of force (F_{act} = -0.24 nN, -0.05 nN, +0.12 nN, and +0.36 nN, top to bottom). B. D_{prot} as a function of F_{act} (cells were all initially submitted to F_{comp}= 0.36 nN). Gray area represents SDs. Each dot represents an average over 7 to 20 cells across 8 experiments. C. Maximal protrusion length ΔL_{max} as a function of its tip diameter D_{prot}, for various applied forces F_{act}. Cells were all submitted to an initial compression F_{comp}= 0.36 nN. Errors bars are SDs. Each dot represents an average over 2 to 12 cells across 8 experiments, except a dot representing a single cell for F_{act} = 0.03 nN. The dashed line is a fit assuming a maximal volume of actin of ~7 µm^3 in the protrusion when reaching its maximal length. D. Volume and surface area of T cells at initial time and when the protrusion was the longest. ****: p<0.0001 for a two-tailed t-test. E. D_{prot} for different values of F_{comp} and F_{act}, and diameter D_{Hertz} of the initial cell-bead contact diameter based on the Hertz model (see methods).

This article is protected by copyright. All rights reserved.

Accepted Article

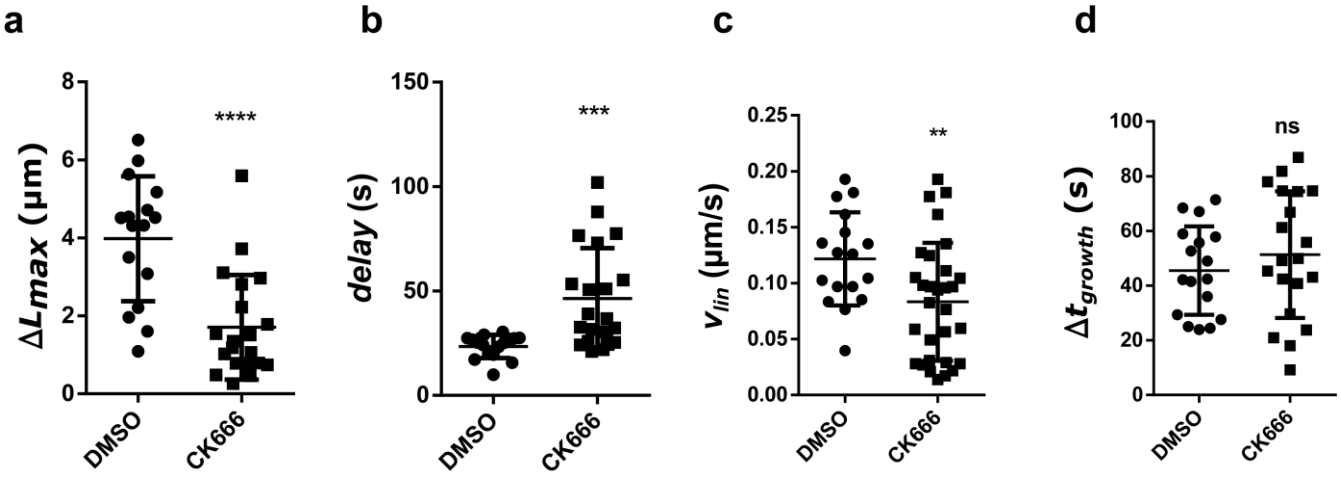

Figure 4. Inhibition of Arp2/3 by CK666 leads to shorter (a), delayed (b), and slower growing (c) T cell protrusions, but does not change growth duration (d). DMSO control: n=2 experiments, N=16 cells; CK666: n=3 experiments, N=20 cells. Statistical tests: 2-tailed unpaired t-tests with Welch correction.

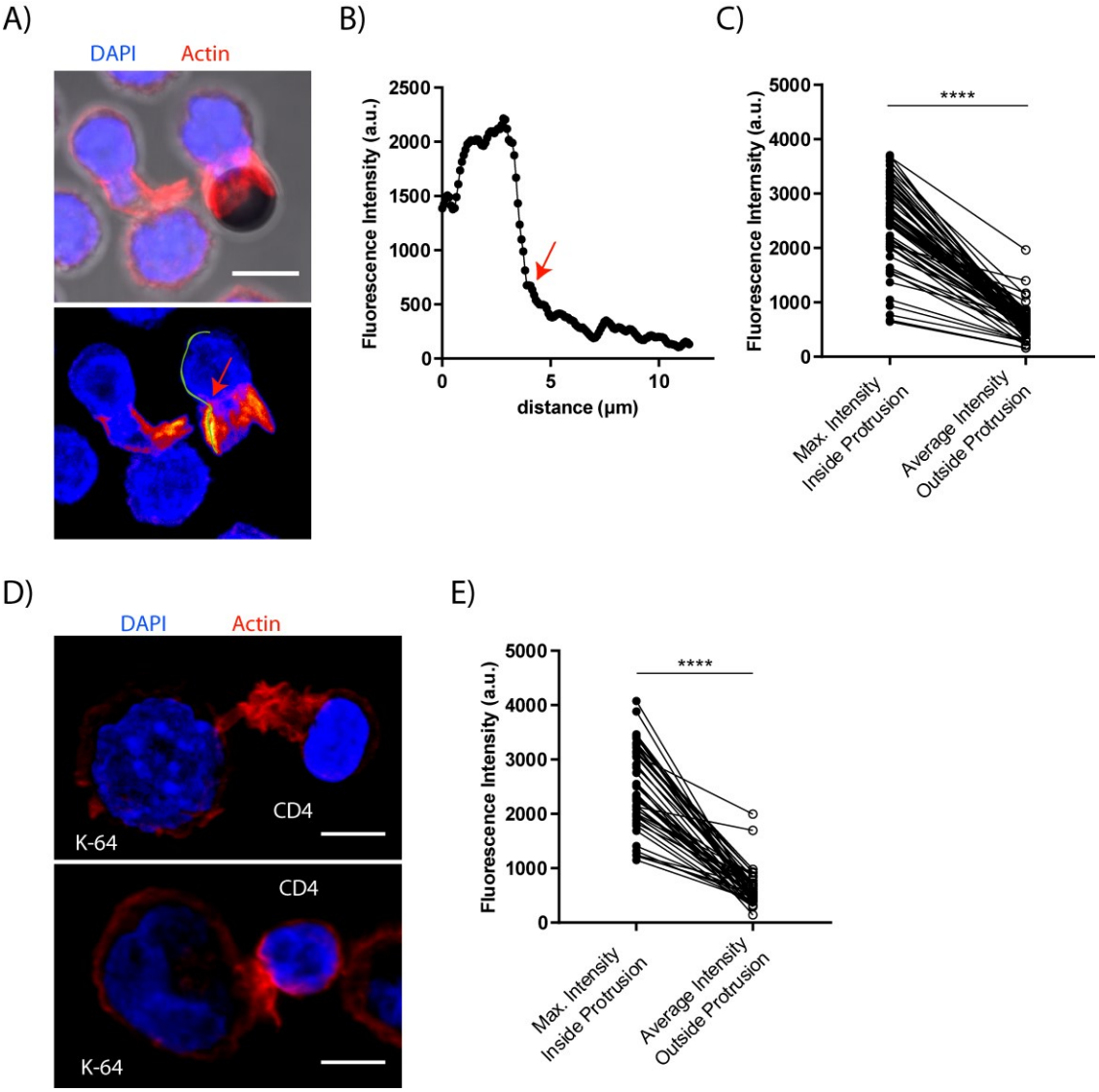

Accepted Article

Figure 5. F-actin organization. A. Top: maximum intensity confocal stack projection (F-actin in red, nucleus in blue, and brightfield in gray). Bottom: only the F-actin image from top is shown using false colors to visualize the enrichment in F-actin in the protrusion walls. A line is drawn on half of the cortical part of the activated cell, the corresponding intensity profile is shown in B. The arrow indicates the base of the protrusion. Scale bar is 5 µm. B. Fluorescence intensity along the line drawn in A. The distance is counted starting from the bead towards the back of the cell. The arrow corresponds to the base of the protrusion. C. Fluorescence intensity of F-actin in the cortex of primary T cells activated by a bead. For each cell, the average intensity in the protrusion was compared to the average intensity in the cortex located outside the protrusion. Each dot represents a single cell (N=83 cells, n=2 experiments, Wilcoxon matched-pairs signed rank test). D. Two examples of protrusions between a primary T-lymphocyte and a K64 cell. F-actin is shown in red for both cells and the K64 cells are shown in blue. E. Fluorescence intensity analyzed as in C, the average intensity in the protrusion was compared to the average intensity in the cortex located outside the protrusion in T cells in contact with K-64 cells (each dot represents a T cell, N=50 cells across n=2 experiments, two-tailed t-test).

Graphical Abstract

During Immunological Synapse formation, T cells emit an actin-rich protrusion that experiences forces. Here, we quantitavely characterized the effects of external forces in the dynamic of the protrusion. We found that the formation of the protrusion is set by an intracellular constant time and is mediated by the Arp2/3 complex and that its dynamic is sensitive to external forces. Our study provides key insights that help to better understand the mechanism involved in the formation of the actin protrusion emited by the T-cell.

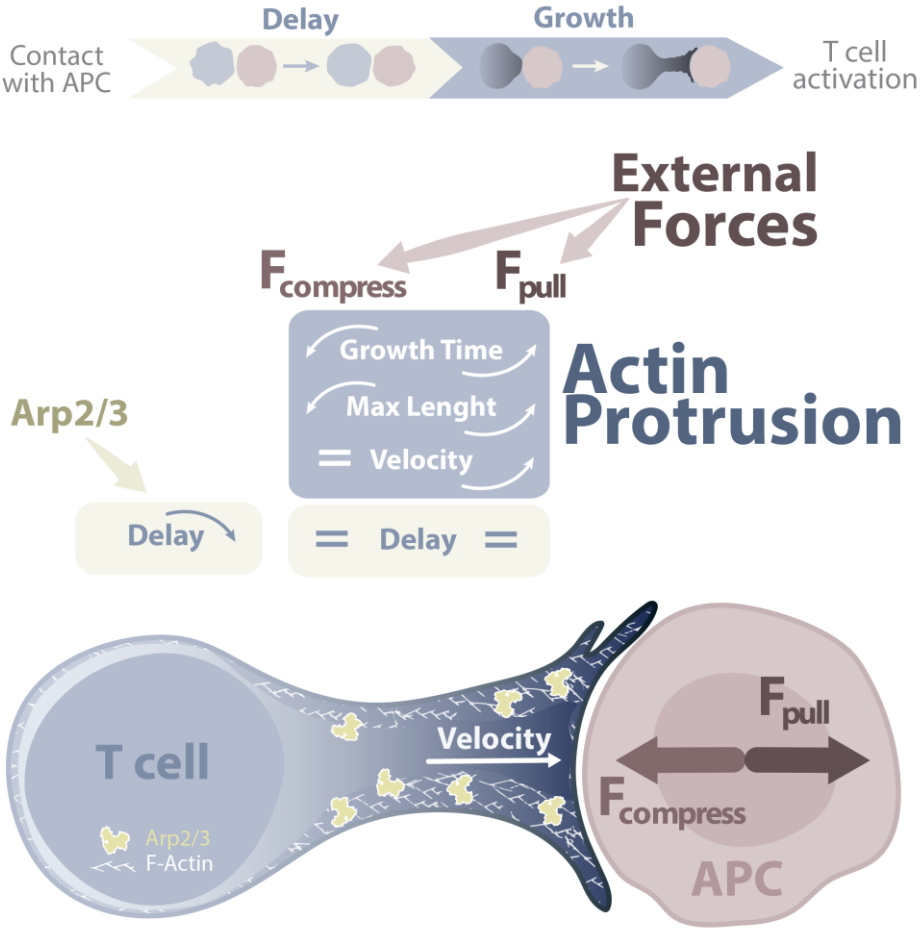

This article is protected by copyright. All rights reserved.